PAPER

Check for updates

Poly(ethylene glycol)-functionalized 3D covalent organic frameworks as solid-state polyelectrolytes†

Miaomiao Wu, [ID] ‡ Hongrui Huang,‡ Bingqing Xu* and Gen Zhang [ID] *

Existing lithium-ion-conducting covalent organic frameworks (COFs) are mainly two-dimensional, in which the one-dimensional channels are difficult to completely and uniformly stack in the same direction, particularly in the case of powdered COFs, resulting in the hindrance of ion transport at the grain boundary or at the interface of the powder contact. In this contribution, poly(ethylene glycol) (PEG)-functionalized three-dimensional COFs with 3D channels were successfully constructed for ion conduction in different directions, which is conducive to reducing the grain boundary and interface contact resistance. Combined with the coupling behaviour between the PEG chain segments and Li-ions, the 3D COF incorporated with LiTFSI achieves a high ionic conductivity of 3.6×10^{-4} S cm^{-1} at 260 °C. The maximum operating temperature is higher than the boiling point of commercial organic electrolytes, indicating the excellent security of PEG-based COFs as Li-ion polyelectrolytes at high temperature.

Lithium-ion batteries (LIBs) are an indispensable energy storage system in contemporary society,[1–3] but most of them use liquid electrolytes, posing the risk of flammability, particularly in large-scale applications.[4,5] Solid electrolytes have been explored as ideal substitutes,[6–12] which commonly encompass ether polymeric- or ceramic-based electrolytes. Nonetheless, ceramic electrolytes still encounter large obstacles, such as instability, poor processability, and non-negligible grain boundary resistance.[8,13,14] Polymer electrolytes have higher stability and lower interfacial resistance, and are considered to be more promising polyelectrolyte materials. In particular, poly(ethylene glycol) (PEG)-based polymers, which are constructed by grafting PEG onto polymer chains, possess considerable ionic conductivity. However, they undergo a solid-to-liquid translation process with increasing temperature,[15] which can easily cause a short circuit between the cathode and anode from the electrolyte draining, leading to acute safety risks. It is also laborious to expound the structure–property relationship between the ion-conducting pathways and ion conduction due to the structurally disordered character of PEG-based electrolytes.[16]

Covalent organic frameworks (COFs) are a novel class of Li-ion conducting materials, which can acquire superior

chemical, thermal and electrochemical stability through certain organic bonds or robust π–π stacking.[17–22] Compatible COFs can not only provide precisely tuned spatial pores for ion transport but also provide insight into the conduction mechanisms based on the long-range order.[23–26] The existing COF-based electrolytes are mainly divided into three categories: (i) COFs with non-electric neutral skeletons (Li-ion as the equilibrium cation), which need an external organic solvent to support ion transport, posing similar safety problems as organic liquid electrolytes;[27,28] (ii) COFs doped with PEG and lithium salt, in which the physically adsorbed PEG has a leakage risk;[15] and (iii) PEG-functionalized COFs, of which the powder has anisotropy, resulting in disappointing ionic conductivity.[29–31] To the best of our knowledge, most of the existing Li-ion-conducting COFs are two dimensional, in which the one-dimensional channels can hardly be completely and uniformly stacked in the same direction, especially in the case of the powder-form COFs, which will lead to blockage of ion transport at the grain boundary or at the interface of the powder contact.

In view of this, we have developed a self-assembly strategy to construct a PEG-functionalized three-dimensional COF, which has more ion transport paths in different directions that are beneficial to reducing the grain boundary and interface contact resistance experienced in the bulk condition. Distinct from amorphous bulk PEG, the grafted PEG constructs clear Li$^+$-conducting routes in crystalline frameworks, which is beneficial to understanding the relationship between structure and ionic conduction. PEG with small molecular weight exhibits a liquid

Key Laboratory for Soft Chemistry and Functional Materials of Ministry of Education, School of Chemistry and Chemical Engineering, Nanjing University of Science and Technology, Nanjing, Jiangsu 210094, China. E-mail: zhanggen@njust.edu.cn

‡ These authors contributed equally.

state at room temperature, but the hybrid materials consisting of short-chain PEG and COFs macroscopically present a solid state due to the confinement of the rigid skeleton of the COFs. The highest operating temperature can reach 260 °C along with a remarkable ionic conductivity of 3.6×10^{-4} S cm^{-1}. This temperature is higher than the boiling point of commercial organic electrolytes such as propylene carbonate (242 °C), diethyl carbonate (127 °C) and dimethyl carbonate (91 °C),

indicating the excellent security of PEG-based COFs as Li-ion electrolytes.

In this work, three types of PEG-functionalized COFs were synthesized under solvothermal conditions by the condensation of tetrakis(4-aminophenyl)methane with three aldehyde monomers with different lengths of PEG chains (Fig. 1a). The corresponding three-dimensional COFs, denoted as 3D-COF-PEG2, 3D-COF-PEG3 and 3D-COF-PEG6 hereafter, were produced as microcrystalline powders insoluble in common organic solvents. 3D-COF-PEG2-Li, 3D-COF-PEG3-Li and 3D-COF-PEG6-Li were prepared by introducing LiTFSI into the COFs.

The crystallinity of the COFs was evaluated by PXRD, and due to the structural consistency of these samples, 3D-COF-PEG2 was taken out to build in Materials Studio. The PXRD pattern of 3D-COF-PEG2 with its simulated value is illustrated in Fig. 1b, showing that it possessed a *dia* topology with 5-fold interpenetration, and it could be observed that the obvious peaks at 4.24° along with few weaker peaks at 6.13° and 8.63° corresponded to the (220), (040) and (440) planes with the *FDDD* (70) space group. The negligible values of $R_{wp} = 2.78\%$ and $R_p = 2.11\%$ imply that the Pawley refinement of the 3D-COF-PE2 pattern coincides with the experimental pattern. There are no diffraction peaks after modification with LiTFSI (Fig. S1, ESI†), which is due to the disordered LiTFSI and ion-coupled PEG chains in the channel. The three-dimensional compounds are connected by imine bonds, and the structures are shown in Fig. 1c.

For the isomorphic compounds, the PXRD of the three samples are consistent (Fig. 2a). Their morphology reveals uneven spherical and elliptical shapes, as seen in the SEM images (Fig. 3). It could be seen that the maximum nitrogen adsorption values are 133, 102 and 101 cm^3 g^{-1} for 3D-COF-PEG2, 3D-COF-
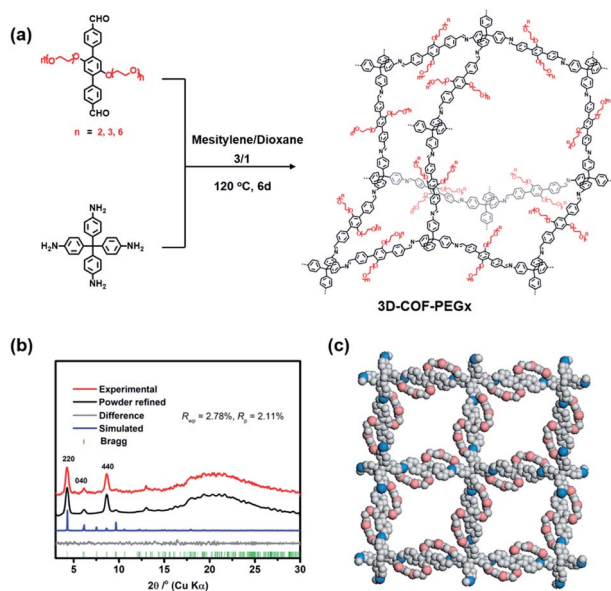

Fig. 1 (a) A bottom-up strategy for the synthesis of COFs. (b) Observed PXRD patterns of 3D-COF-PEG2: experimental PXRD pattern (black line), Pawley-refined pattern (red line), calculated pattern (blue line), and their difference (green line). (c) *dia* topology structure of 3D-COF-PEG2.
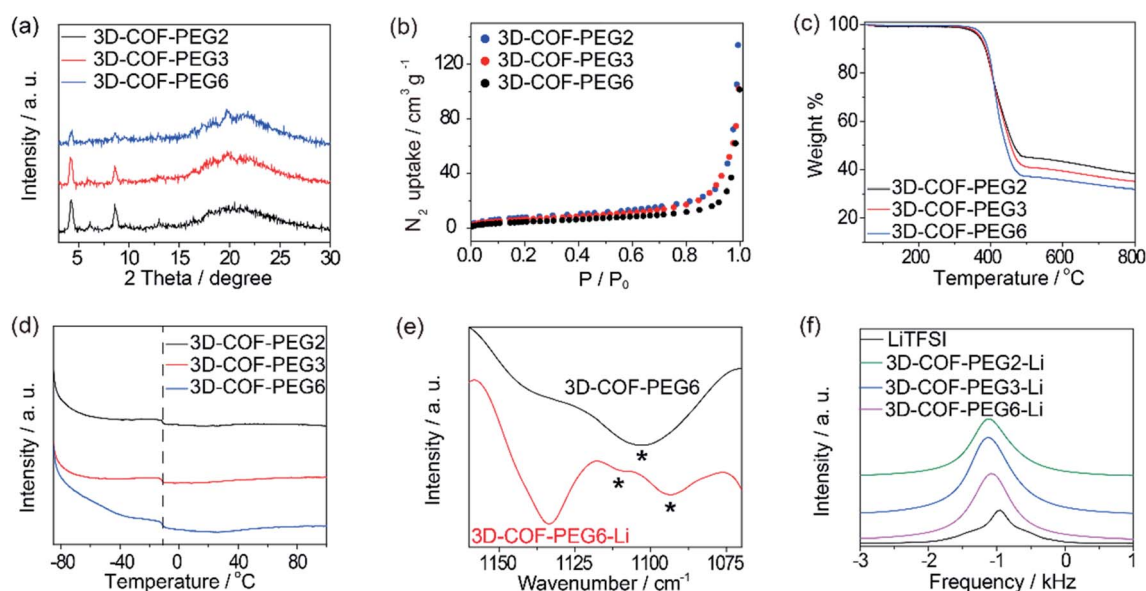

Fig. 2 (a) PXRD patterns, (b) N$_2$ adsorption, (c) TG plots and (d) DSC curves of 3D-COF-PEG2, 3D-COF-PEG3 and 3D-COF-PEG6. (e) IR plots of 3D-COF-PEG6 and 3D-COF-PEG6-Li. (f) ^{7}Li solid NMR for LiTFSI, 3D-COF-PEG2-Li, 3D-COF-PEG3-Li and 3D-COF-PEG6-Li.
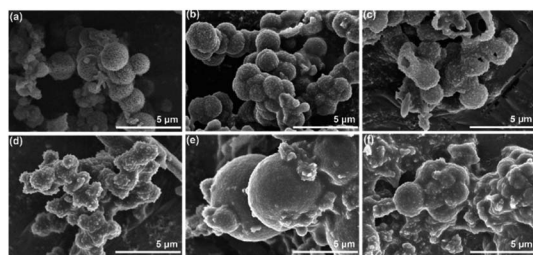
Fig. 3 (a–c) SEM patterns of 3D-COF-PEG2, 3D-COF-PEG3 and 3D-COF-PEG6, respectively. (d–f) SEM patterns of 3D-COF-PEG2-Li, 3D-COF-PEG3-Li and 3D-COF-PEG6-Li, respectively.

PEG3 and 3D-COF-PEG6, respectively, proving a more crowded situation in 3D-COF-PEG6 (Fig. 2b). After introducing LiTFSI, the adsorption amounts clearly drop to 71.0, 39.8 and 79.2 cm^3 g^{-1} for 3D-COF-PEG2-Li, 3D-COF-PEG3-Li and 3D-COF-PEG6-Li, respectively (Fig. S2, ESI†). The thermal stability and thermodynamics were also analysed. There is almost no weight loss before 400 °C for these COFs before or after introducing LiTFSI, demonstrating their remarkable thermal stability (Fig. 2c and S3, ESI†). As seen in Fig. 2d, three COFs exhibit an endothermic peak at −11 °C in the measured temperature region, showing a segment movement behaviour, which is conducive to ionic conduction (Fig. S4, ESI†). From the IR plots (Fig. 2e), it can be seen that there is a single ν_{as}(COC) peak at 1103 cm^{-1} for 3D-COF-PEG6, but it splits into two peaks for 3D-COF-PEG6-Li at 1109 cm^{-1} and 1093 cm^{-1} (Fig. 2e). This is similar to the other samples, implying an interaction between Li$^+$ and the PEG chains (Fig. S5, ESI†). The ^{7}Li NMR peaks are located at −946 Hz, −1106 Hz, −1126 Hz and −1074 Hz for bulk LiTFSI, 3D-COF-PEG2-Li, 3D-COF-PEG3-Li and 3D-COF-PEG6-

Li, respectively, showing a unique chemical state of the Li ions in the COFs (Fig. 2f).

The ionic conductivity (σ) was calculated from the Nyquist plots *versus* different temperatures (Fig. 4a and S6–S8, ESI†). The σ of 3D-COF-PEG2-Li is 8.5×10^{-9} S cm^{-1} at 100 °C, 1.2×10^{-6} S cm^{-1} at 180 °C and 1.2×10^{-5} S cm^{-1} at 260 °C. 3D-COF-PEG3-Li exhibits higher ionic conductivity values of 3.4×10^{-8} S cm^{-1} at 100 °C, 4.5×10^{-6} S cm^{-1} at 180 °C, and 5.3×10^{-4} S cm^{-1} at 260 °C. The ionic conductivity of 3D-COF-PEG6-Li is the highest, at 3.7×10^{-6} S cm^{-1} at 100 °C, 7.0×10^{-5} S cm^{-1} at 180 °C, and 3.6×10^{-4} S cm^{-1} at 260 °C (Fig. 4b). Obviously, with an increase in the length of the PEG chain, the ionic conductivity climbs as well, because of which the longer PEG chain offers more coupling sites for lithium ions to facilitate the ionic conduction. Furthermore, the highest operating temperature (260 °C) is higher than the boiling point of commercial organic electrolytes such as propylene carbonate (242 °C), diethyl carbonate (127 °C), and dimethyl carbonate (91 °C), indicating the excellent safety of PEG-based COFs as Li-ion electrolytes. The long-term ionic conduction durability measurement of 3D-COF-PEG6-Li was also carried out at 200 °C for 42 h (Fig. 4c). It affords stable conductivity above ∼10^{-4} S cm^{-1}, demonstrating its prominent ionic conductivity retention. The activity energy value (E_a) is calculated to be around 0.49 eV for 3D-COF-PEG6-Li, which is smaller than those of 3D-COF-PEG2-Li and 3D-COF-PEG3-Li (0.78 eV and 0.79 eV, respectively) (Fig. 4d and S9, ESI†), showing the lower Li$^+$ conducting energy barrier in COF-PEG-B6-Li. With longer PEG chains, the coupling behaviour between ether bonds and lithium ions will be more frequent, which is one important cause of the decreased Li$^+$ conduction barrier. As illustrated in Fig. 4e, the Li$^+$ transference number is around 0.22 for COF-
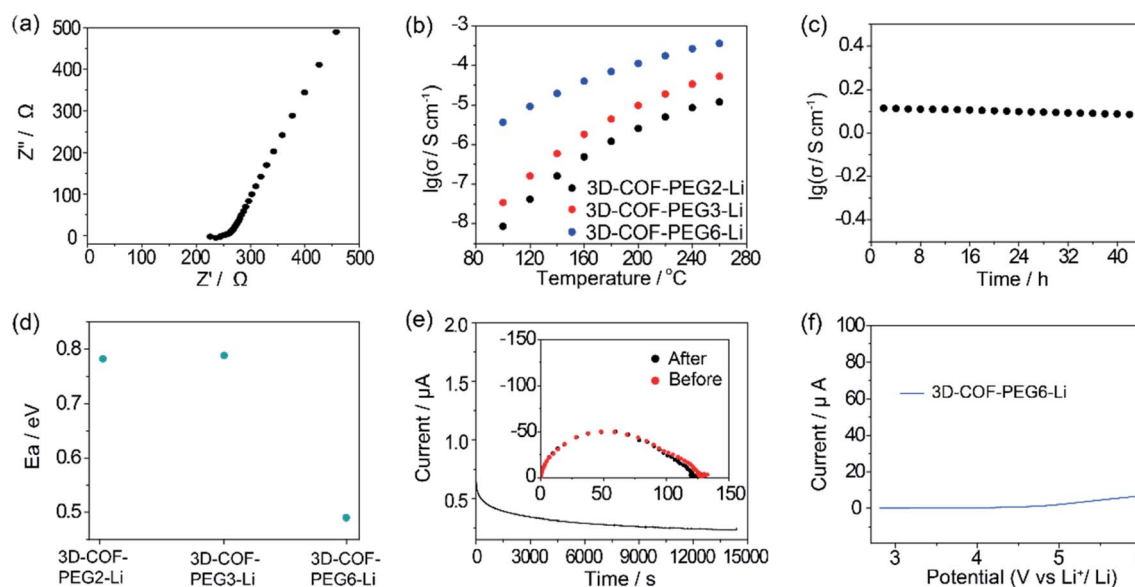

Fig. 4 (a) Nyquist plots of 3D-COF-PEG6-Li at 260 °C. (b) Ionic conductivity of 3D-COF-PEG2-Li, 3D-COF-PEG3-Li and 3D-COF-PEG6-Li *versus* temperature from 100 °C to 260 °C. (c) Long-term ionic conducting durability test of 3D-COF-PEG6-Li at 200 °C. (d) Calculation of activation energy for 3D-COF-PEG2-Li, 3D-COF-PEG3-Li and 3D-COF-PEG6-Li. (e) Li$^+$ transference number measurement of 3D-COF-PEG6-Li at 100 °C. (f) Linear sweep voltammograms (LSV) of 3D-COF-PEG6-Li at 100 °C.

PEG-B6-Li at 100 °C, which is comparable to that of PEG-based polymer electrolytes. COFs introduced with LiTFSI also show high electrochemical stability, and they are all stable when the voltage is lower than 4 V, suggesting their compatibility with high voltage cathodes (Fig. 4e and S10, ESI†).

Conclusions

To sum up, we have developed a self-assembly strategy to construct PEG-functionalized three-dimensional COFs for the first time, possessing more transmission paths for ion transport in different directions, which is beneficial to reducing the grain boundary and interface contact resistance found in the bulk condition. Combined with the coupling behaviour between PEG chains and Li-ions, the 3D COF incorporated with LiTFSI achieves the highest ionic conductivity of 3.6×10^{-4} S cm^{-1} at 260 °C. The highest operating temperature is higher than the boiling point of commercial organic electrolytes, indicating the excellent security of PEG-based COFs as Li-ion electrolytes. This study contributes a new strategy to construct high-performance PEG-based polyelectrolytes for next-generation solid lithium batteries.

Author contributions

The manuscript was written through the contribution of all authors. All authors have given their approval to the final version of the manuscript.

Conflicts of interest

The authors declare no competing financial interest.

Notes and references

1 W. Li, B. Song and A. Manthiram, *Chem. Soc. Rev.*, 2017, **46**, 3006–3059.

2 J. B. Goodenough and Y. Kim, *Chem. Mater.*, 2010, **22**, 587–603.

3 N. Kamaya, K. Homma, Y. Yamakawa, M. Hirayama, R. Kanno, M. Yonemura, T. Kamiyama, Y. Kato, S. Hama, K. Kawamoto and A. Mitsui, *Nat. Mater.*, 2011, **10**, 682–686.

4 M. Armand and J. M. Tarascon, *Nature*, 2008, **451**, 652–657.

5 C. Sun, J. Liu, Y. Gong, D. P. Wilkinson and J. Zhang, *Nano Energy*, 2017, **33**, 363–386.

6 Z. Gadjourova, Y. G. Andreev, D. P. Tunstall and P. G. Bruce, *Nature*, 2001, **412**, 520–523.

7 F. Croce, G. B. Appetecchi, L. Persi and B. Scrosati, *Nature*, 1998, **394**, 456–458.

8 A. Manthiram, X. Yu and S. Wang, *Nat. Rev. Mater.*, 2017, **2**, 16103.

9 M. A. Kraft, S. Ohno, T. Zinkevich, R. Koerver, S. P. Culver, T. Fuchs, A. Senyshyn, S. Indris, B. J. Morgan and W. G. Zeier, *J. Am. Chem. Soc.*, 2018, **140**, 16330–16339.

10 Y. Zhao and L. L. Daemen, *J. Am. Chem. Soc.*, 2012, **134**, 15042–15047.

11 J. Janek and W. G. Zeier, *Nat. Energy*, 2016, **1**, 16141.

12 Y. Kato, S. Hori, T. Saito, K. Suzuki, M. Hirayama, A. Mitsui, M. Yonemura, H. Iba and R. Kanno, *Nat. Energy*, 2016, **1**, 16030.

13 L. Shen, H. B. Wu, F. Liu, J. L. Brosmer, G. Shen, X. Wang, J. I. Zink, Q. Xiao, M. Cai, G. Wang, Y. Lu and B. Dunn, *Adv. Mater.*, 2018, **30**, 1707476.

14 J. C. Bachman, S. Muy, A. Grimaud, H.-H. Chang, N. Pour, S. F. Lux, O. Paschos, F. Maglia, S. Lupart, P. Lamp, L. Giordano and Y. Shao-Horn, *Chem. Rev.*, 2016, **116**, 140–162.

15 Z. Guo, Y. Zhang, Y. Dong, J. Li, S. Li, P. Shao, X. Feng and B. Wang, *J. Am. Chem. Soc.*, 2019, **141**, 1923–1927.

16 M. Sadakiyo, T. Yamada, K. Honda, H. Matsui and H. Kitagawa, *J. Am. Chem. Soc.*, 2014, **136**, 7701–7707.

17 S.-Y. Ding and W. Wang, *Chem. Soc. Rev.*, 2013, **42**, 548–568.

18 C. S. Diercks and O. M. Yaghi, *Science*, 2017, **355**, eaal1585.

19 J. Li, X. Jing, Q. Li, S. Li, X. Gao, X. Feng and B. Wang, *Chem. Soc. Rev.*, 2020, **49**, 3565–3604.

20 Y. An, S. Tan, Y. Liu, K. Zhu, L. Hu, Y. Rong and Q. An, *Energy Storage Mater.*, 2021, **41**, 354–379.

21 Y. Jiang, H. Jung, S. H. Joo, Q. K. Sun, C. Li, H.-J. Noh, I. Oh, Y. J. Kim, S. K. Kwak, J.-W. Yoo and J.-B. Baek, *Angew. Chem., Int. Ed.*, 2021, **60**, 17191–17197.

22 Z. Shan, M. Wu, Y. Du, B. Xu, B. He, X. Wu and G. Zhang, *Chem. Mater.*, 2021, **33**, 5058–5066.

23 K. C. Ranjeesh, R. Illathvalappil, S. D. Veer, J. Peter, V. C. Wakchaure, X. Goudappagouda, K. V. Raj, S. Kurungot and S. S. Babu, *J. Am. Chem. Soc.*, 2019, **141**, 14950–14954.

24 Y. Kong, X. He, H. Wu, Y. Yang, L. Cao, R. Li, B. Shi, G. He, Y. Liu, Q. Peng, C. Fan, Z. Zhang and Z. Jiang, *Angew. Chem., Int. Ed.*, 2021, **60**, 17638–17646.

25 G. Zhang, Y.-L. Hong, Y. Nishiyama, S. Bai, S. Kitagawa and S. Horike, *J. Am. Chem. Soc.*, 2019, **141**, 1227–1234.

26 K. Jeong, S. Park, G. Y. Jung, S. H. Kim, Y.-H. Lee, S. K. Kwak and S.-Y. Lee, *J. Am. Chem. Soc.*, 2019, **141**, 5880–5885.

27 Y. Hu, N. Dunlap, S. Wan, S. Lu, S. Huang, I. Sellinger, M. Ortiz, Y. Jin, S.-H. Lee and W. Zhang, *J. Am. Chem. Soc.*, 2019, **141**, 7518–7525.

28 Y. Du, H. Yang, J. M. Whiteley, S. Wan, Y. Jin, S.-H. Lee and W. Zhang, *Angew. Chem., Int. Ed.*, 2016, **55**, 1737–1741.

29 D. A. Vazquez-Molina, G. S. Mohammad-Pour, C. Lee, M. W. Logan, X. Duan, J. K. Harper and F. J. Uribe-Romo, *J. Am. Chem. Soc.*, 2016, **138**, 9767–9770.

30 H. Chen, H. Tu, C. Hu, Y. Liu, D. Dong, Y. Sun, Y. Dai, S. Wang, H. Qian, Z. Lin and L. Chen, *J. Am. Chem. Soc.*, 2018, **140**, 896–899.

31 Q. Xu, S. Tao, Q. Jiang and D. Jiang, *J. Am. Chem. Soc.*, 2018, **140**, 7429–7432.